Available online at www.sciencedirect.com

jmr&t Journal of Materials Research and Technology

www.jmrt.com.br

Original Article

Modeling and computational simulation of fluid flow, heat transfer and inclusions trajectories in a tundish of a steel continuous casting machine

José Renê de Sousa Rocha [a], Emerson Edilson Barros de Souza [a], Francisco Marcondes [a], Jose Adilson de Castro [b,*]

[a] Department of Metallurgical Engineering and Materials Science, Federal University of Ceará Campus do Pici,Ceará, Brazil
[b] Department of Mechanical Engineering, Federal Fluminense University, Rio de Janeiro, Brazil

ARTICLE INFO

Article history:
Received 10 June 2019
Accepted 15 July 2019
Available online 31 July 2019

Keywords:
Numerical simulation
Continuous casting tundish
RTD
Ansys CFX
EbFVM
Inclusion removal

ABSTRACT

Currently, the continuous casting process is the main route used in the integrated steelmaking process. The tundish is an essential component of the caster machine and plays an important role in the control of inclusion in the production of the clean steels. Thus, viable methodologies and predictive models to evaluate this metallurgical reactor efficiency are important technological allies to improve the clean steel production. The main goal of the present study is to develop a computational tool to analyze the turbulent fluid flow, temperature distribution and inclusions removal during the continuous operation of the tundish of an industrial facility to improve its internal configuration. New configurations using weirs and dams are proposed which improve the steel quality. We used the Ansys CFX® software based on the element-based finite-volume method (EbFVM) to solve the coupled turbulent flow and heat transfer model equations in an Eulerian flame. A random nucleation mechanism for the inclusions generation and a modified Lagrangian model with a random walking model (RWM) to account for the effect of turbulence on the inclusions trajectories were proposed. The flow pattern was successfully validated with experimental data. The results were presented in terms of velocity and temperature fields and residence time distribution (RTD) curves. Then, the model was used to investigate new scenarios and enhanced geometry configurations.

1. Introduction

Nowadays, the continuous casting process is the most used technique to produce semi-finished steel. To attain steel cleanliness, one of the most important devices employed in this process is the tundish reactor. In the last decades, the tundish has been designed not only to be an intermediate vessel between the ladle and the mold, but also an inclusion removal and a metallurgical reactor. As non-metallic inclusion density is about half of liquid steel density, they can be removed captured in the slag layer protection, when they reach it by a flotation mechanism. If inclusion particles remain into the molten steel on a certain level of concentration or size, they may produce several defects in the semi-finished products, lending to troubleshooting during the finishing mill process.

* Corresponding author.
E-mail: joseadilsoncastro@id.uff.br (J.A. Castro).
https://doi.org/10.1016/j.jmrt.2019.07.029

Nomenclature

C	dimensionless concentration
C_D	drag coefficient
C_p	specific heat at constant pressure (J/(kg K))
$C_{\varepsilon 1}$	constant for k–ε turbulence model
$C_{\varepsilon 2}$	constant for k–ε turbulence model
C_μ	constant for k–ε turbulence model
D	kinematic diffusivity (m^2/s)
D_{eff}	effective kinematic diffusivity (m^2/s)
d_p	diameter of the particle (m)
h	enthalpy (m^2/s^2)
k	turbulence kinetic energy (m^2/s^2)
K	thermal conductivity (W/(m K))
K_{eff}	effective thermal conductivity (W/(m K))
m_p	mass particle (kg)
p	pressure (Pa)
P_k	turbulence production (kg/(m s^3))
Pr_t	turbulent Prandtl number
Re	Reynolds number
S_c	turbulent Schmidt number
U_j	fluid velocity (m/s)
U_p	velocity particle (m/s)
ε	turbulence eddy dissipation (m^2/s^3)
$\bar{\theta}$	dimensionless mean time
$\bar{\theta}_C$	dimensionless mean time from $\theta = 0$ to $\theta = 2$
μ	dynamic viscosity (kg/(m s))
μ_{eff}	effective viscosity (kg/(m s))
μ_t	turbulent viscosity (kg/(m s))
ρ	density (kg/m^3)
ρ_p	density of the particle (kg/m^3)
σ_k	constant for k–ε turbulence model
σ_ε	constant for k–ε turbulence model

To increase the cleanness of the steel during the continuous casting process, researchers have carried out investigations using both experimental and numerical approaches, addressing the relevant aspects that govern the fluid flow and heat transfer into the tundish [1–4]. However, experimental analysis has many drawbacks, such as high cost of equipment and less possibility to both change and analyze different scenarios. On the other hand, the numerical analysis of continuous casting processes allows the systematic investigation and optimization of the desirable features.

In this work, the tundish investigation will be performed through the Ansys CFX. Ansys CFX®, which uses the Element-based Finite-Volume Method (EbFVM), combined with an advanced solver and a pre and post-processing powerful tools. Also, finite-volume method is recognized as an approach that can guarantee local conservation of the physical quantities (mass, momentum, energy), a suitable feature for modeling the complex turbulent coupled flow within the tundish reactor [5].

To minimize the inclusions at the tundish, flow control devices have been added to the tundish to control the flow pattern. They can promote flotation of the non-metallic inclusions [6]. Among the fluid flow modifiers, we can cite dams, weirs, stoppers rods, turbulence inhibitors, and gas injectors. In the present study, we used dams and weirs to enhance the inclusion removal from the tundish. The weir can guarantee low intensity of turbulence at the slag layer; however, it cannot eliminate short-circuiting in a given tundish. Unlike the weir, the dam can eliminate short-circuiting completely; also, it has some others desired features such as the creation of surface directed flows, the increase in the mean residence time, and the trap of higher turbulent velocity values at the inlet region [2].

To characterize the fluid flow into the tundish, a specific model must be applied with the information for each fluid element available by the residence time distribution (RTD) curve. This distribution curve is originated from the fact that some fluid element spends more time within the tundish than others [6]. In the present study, we used the combined or mixed model [2]. This model divided the whole fluid volume of the tundish in three volumes: dispersed plug flow volume, well-mixed volume, and dead volume.

Kemeny et al. [7] performed an experimental work of tundishes with and without flow modifiers. The authors investigated optimized locations for dams and weirs based on RTD curves. By modifying the shape of the tundish (T-delta-shaped) and applying just a single barrier, Wollmann et al. [8] observed an increase in the mean residence time; they also addressed ways to eliminate the short-circuiting. Chao Chen et al. [9] studied the inclusion deposition at the steel-slag interface using two tundish designs for different parameters (size of inclusions, steel-slag interfaces, and absorption conditions). The results showed that the tundish with weir and dam exhibited better performance for larger inclusions, while the bare tundish performed better for smaller inclusions. Ning Ding et al. [10] applied physical modeling using the Fluent® CFD software to optimize a tundish with dams and weirs. However, based on their results of velocity and concentration fields, and using RTD curves, they observed an increase in the minimum residence time of about 40%, a decrease in the dead volume of 72%, and also a reduction in the inclusion area ratio of casting slabs by 32%.

Although the fluid flow has a large impact on the inclusion removal of the tundishes, the temperature also has a significant role in this process; therefore, the latter cannot be neglected. Also, as turbulence is decreased from inlet to the bulk fluid region, buoyant forces become predominant in these regions, and hence natural convection promotes the flotation of non-metallic inclusions [11]. The non-isothermal behavior of molten steel into the tundish may cause significant changes in the mean residence time, temperature distribution, and inclusion movements [12]. Alizadeh et al. [13] carried out a steady state water modeling analysis under non-isothermal conditions in a twin-slab-strand continuous casting tundish. Their results showed that RTD curves were completely different under isothermal and non-isothermal conditions. They explained the difference due to the presence of mixed convection phenomena in the non-isothermal tundish. De Kock [14] performed both a plant trial and a water model study in conjunction with numerical analysis in various types of tundishes. He aimed to obtain RTD curves as well as temperature distribution in non-isothermal tundishes to achieve an optimum design for each configuration. One of his results using weir and dam configuration was the minimization of the

dead volume and the maximization of the inclusion removal into the tundish.

Generally, tundishes without any flow modifiers allow strong boundaries effects, and hence the spatial temperature becomes nonuniformly. When adding some kind of flow control, the heat loss is reduced, and then the temperature field must become more uniform [15]. Raghavendra et al. [16] studied the influence of thermal induced flows for inclusion flotation. The well-known open source CFD code, OpenFOAM, was used for modeling inclusion path in a four-strand asymmetric billet caster tundish. They obtained different fractions of removed particles when comparing isothermal and non-isothermal cases. Sowa [17] performed a numerical investigation of some flow devices considering the changes of thermophysical properties with the temperature. It was concluded that the velocity of the molten steel has a significant influence on the temperature field because the motion near the slag layer causes the formation of dead zones and local temperature drop.

As the inclusions are particles with distinguishable mass, they are elements that can be followed to analyze their behavior into the computational domain. For this case, the Lagrangian analysis can be applied to describe the nonmetallic inclusions paths. Miki and Thomas [18] evaluated the influence of the Random Walk Model (RWM) in the trajectory of inclusions. They concluded that the chaotic fluctuation due to the turbulence enhances the flotation of small inclusions. On the other hand, this random motion also causes particle collisions, then promoting a decrease in the fast removal of large inclusions.

In the present study, we propose a comprehensive mathematical model and numerical analysis of the fluid flow and temperature fields into an actual tundish configuration. Additionally, we newly propose a both Eulerian and Lagrangian approaches for modeling the inclusion generation, motion capture based on a random noise inclusion to account for the turbulence effects on the trajectories. The turbulence quantities were calculated using the k–ε and SST models.

2. Model formulation

Herein, we present the equations used to model the fluid flow and heat transfer into the tundish, as well as, the turbulence model employed to evaluate the turbulence quantities. We also show the tracer concentration equation and the Lagrangian equation to obtain the fraction of particles at the slag cover. The fluid flow into the tundish was treated as a 3D turbulent and incompressible fluid flow. Constant values of the physical properties for steel and water were used to model the molten steel into the tundish for both isothermal and non-isothermal cases. The AISI 1025 steel properties were used for the non-isothermal simulations [14,19,20,28]. The slag layer was assumed to be flat and had a constant bath height.

Furthermore, the secondary reaction in both slag layer-air and slag layer-molten steel interface was neglected. The heat loss due to radiation and convection were incorporated in heat fluxes at slag layer as well as for the lateral and bottom walls of the tundish, whereas the dams and weirs were assumed to be adiabatic. The effects of collision, coalescence, and reoxidation of particles as well as sticking to the walls are not accounted for the Lagrangian analysis. Also, spherical particles with a specified diameter and having a constant density of 4000 kg/m^3 are employed. The tracer is treated as a passive scalar, meaning that its path throughout the tundish does not influence the flow field.

2.1. Continuity and momentum equations

The continuity and momentum equations after averaging the continuity and momentum equations and using the Boussinesq eddy-viscosity approximation to relate the Reynolds stresses to the strain rate of the mean motion are given by:

$$\frac{\partial \rho}{\partial t} + \frac{\partial (\rho U_j)}{\partial x_j} = 0, \tag{1}$$

$$\frac{\partial}{\partial t}(\rho U_i) + \frac{\partial}{\partial x_j}(\rho U_i U_j) = -\frac{\partial p}{\partial x_i} + \frac{\partial}{\partial x_j}\left[\mu_{eff}\left(\frac{\partial U_i}{\partial x_j} + \frac{\partial U_j}{\partial x_i}\right)\right] - \rho_{ref} g \beta (T - T_{ref}), \tag{2}$$

where ρ is the fluid density, U_j are the velocity components, p is the pressure, ρ_{ref} is a reference density, g is the gravitational acceleration, T is the temperature, T_{ref} is a reference temperature, and μ_{eff} is the effective viscosity, which is defined as:

$$\mu_{eff} = \mu + \mu_t, \tag{3}$$

where μ is the dynamic viscosity and μ_t is the turbulent viscosity.

For modeling turbulence quantities, the k–ε model, as well as the SST model, was used, thereby two additional variables were introduced to the previous system of equations.

2.2. k–ε turbulence model

The k–ε model assumes that the turbulence viscosity is related to the turbulence kinetic energy k and the turbulence eddy dissipation ε by the following relation:

$$\mu_t = C_\mu \rho \frac{k^2}{\varepsilon}, \tag{4}$$

where the values of k and ε are calculated by the two following transport equations:

$$\frac{\partial (\rho k)}{\partial t} + \frac{\partial}{\partial x_j}\left(\rho U_j k - \frac{\mu_{eff}}{\sigma_k}\frac{\partial k}{\partial x_j}\right) = P_k - \rho\varepsilon, \tag{5}$$

$$\frac{\partial (\rho \varepsilon)}{\partial t} + \frac{\partial}{\partial x_j}\left(\rho U_j \varepsilon - \frac{\mu_{eff}}{\sigma_\varepsilon}\frac{\partial \varepsilon}{\partial x_j}\right) = \frac{\varepsilon}{k}(C_{\varepsilon 1} P_k - C_{\varepsilon 2}\rho\varepsilon), \tag{6}$$

where C_μ, $C_{\varepsilon 1}$, $C_{\varepsilon 2}$, σ_k, σ_ε are constants taken from Launder and Spalding [20] and P_k is the turbulence production owing to viscous forces. The equations for the turbulence model SST (shear stress transport) can be found elsewhere [19,21,23].

2.3. Tracer convection-diffusion equation

To obtain the RTD curve, it is necessary to solve the tracer diffusion equation that is given by:

$$\frac{\partial}{\partial t}(\rho C) + \frac{\partial}{\partial x_j}(\rho U_j C) = \frac{\partial}{\partial x_j}\left(D_{\text{eff}}\frac{\partial C}{\partial x_j}\right), \tag{7}$$

where C is the tracer concentration and D_{eff} is the effective kinematic diffusivity, which is defined as:

$$D_{\text{eff}} = \rho D + \frac{\mu_t}{S_c}, \tag{8}$$

where D is the kinematic diffusivity and S_c is the turbulent Schmidt number.

2.4. Thermal energy equation

Neglecting the radiative and viscous dissipation effects for incompressible flow, the energy equation in terms of enthalpy (h) is given by:

$$\frac{\partial}{\partial t}(\rho h) + \frac{\partial}{\partial x_j}(\rho U_j h) = \frac{\partial}{\partial x_j}\left(k_{\text{eff}}\frac{\partial T}{\partial x_j}\right), \tag{9}$$

where the effective thermal conductivity (k_{eff}) is defined in terms of the thermal conductivity (k), the specific heat at constant pressure (C_P), and the turbulent Prandtl number (P_{rt}) by:

$$k_{\text{eff}} = k + \frac{C_p \mu_t}{Pr_t}. \tag{10}$$

2.5. Particle tracking model

Each non-metallic inclusion is treated as a small number of particulates immersed in the fluid domain (Lagrangian modeling). In this formulation, particle tracking is performed through a force balance, acting in each particle. Applying a force balance on each particle and accounting for only drag and buoyancy forces, since they represent the main forces on the particles [24], the inclusion path can be described as:

$$m_p \frac{dU_p}{dt} = \frac{1}{8}\pi d_p^2 \rho C_D |U - U_p|(U - U_p) + \frac{1}{6}\pi d_p^3(\rho_p - \rho)g, \tag{11}$$

where m_p denotes the mass of the individual particle and U_p represents the components of the velocities of the particle, meanwhile U represents the liquid local velocities components. The first term on the right-hand side considers the aerodynamic drag forces, where the drag coefficient C_D is given by:

$$C_D = \max\left(\frac{24}{Re}\left(1 + 0.15Re^{0.687}\right), 0.44\right), \tag{12}$$

and the particle Reynolds number is defined as:

$$\text{Re} = \frac{\rho|U - U_p|d_p}{\mu}. \tag{13}$$

The second term on the right-hand side in Eq. (11) accounts for the buoyancy force. To simulate the random effect of turbulent eddies over the inclusion trajectories, a Random Walk Model (RWM) was used. In this model, the instantaneous velocity fluctuations depend on the local level of turbulent kinetic energy and a random number distribution between −1 and 1 is locally sorted and used to scale the local Kinect energy contribution to the particle fluctuation velocities components. Further details on this model can be found elsewhere [22-26].

Table 1 – Physical and operating parameters for validation cases.

Parameters	Case I	Cases II and III
Volume – m^3	4.39	1.8
Inlet diameter – m	0.051	0.065
Outlet diameter – m	0.076	0.036
Inlet mass flow rate – kg/s	3.82	0.83

2.6. Boundary and initial conditions

At the inlet, we prescribed the normal velocity, temperature, and turbulence intensity as 3.57 m/s, 1823 K and 5%, respectively. For Lagrangian analysis, particles were injected uniformly with the same velocity of the fluid. At the outlet, the pressure was prescribed (0 Pa), and null normal gradient for all other variables was used. No-slip wall condition, as well as wall functions, was also applied. For the non-isothermal analysis, a prescribed flux of 9000 W/m^2 was set for all walls of the tundish, except for dams and weirs, which were considered to be adiabatic [14]. For modeling the free surface of steel bath, free-slip wall condition was prescribed, and flux of 18,000 W/m^2 was applied [14]. It is worth to mention that the heat losses which were considered through the slag layer and the other walls were a combination of radiation and convection heat transfer. To take advantage of the symmetry of the tundish, only half of the tundish configuration was simulated, and hence at symmetry plane values of the normal velocity component as well as normal gradients to the boundary were set to zero. The flow field obtained from the steady-state analysis was used for solving both the Lagrangian tracking equation and transient tracer advection-diffusion equation to obtain the number of particles removed at the slag layer and RTD curve, respectively. As an initial condition, we set the tracer concentration equal to zero. Null gradient boundary conditions for all tundish regions were applied, except for the inlet region, where a pulse tracer injection was prescribed.

3. Numerical features and parameters

3.1. Physical and operating parameters for all cases

Three validation case studies were analyzed in the present work. Table 1 shows the physical and operating parameters for all validation case studies. Validation case I is an experimental work of Kemeny et al. [7], validation case II is an experimental work of Wollmann [8], and validation case III is a numerical work of Daoud [25]. The latter work used the same geometry and operating parameters of Wollmann [8].

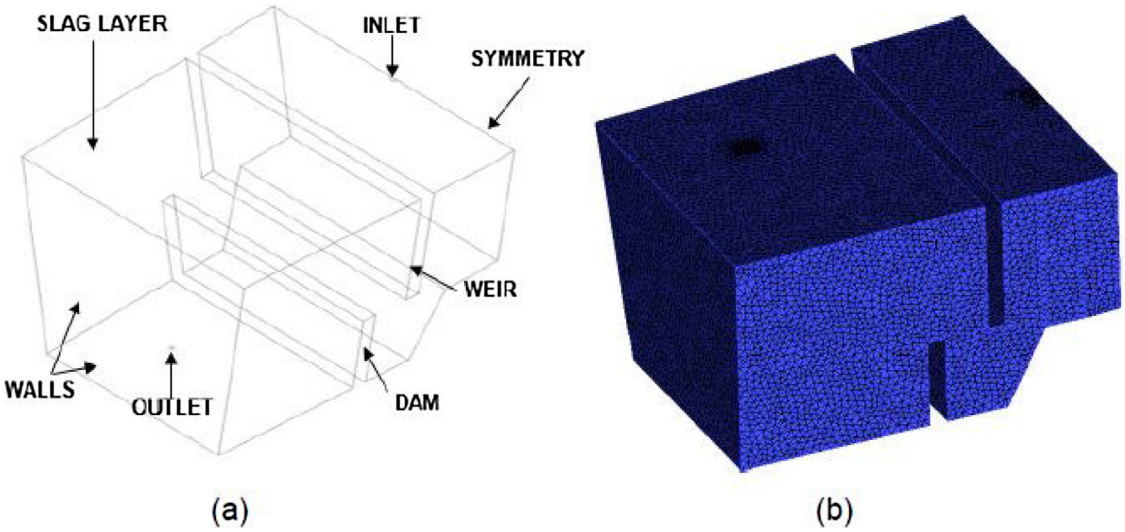

Fig. 1 – Half tundish geometry and mesh: (a) tundish with dam and weir and (b) unstructured mesh.

Table 2 – Physical parameters for numerical analysis.

The case I – volume	0.663 m^3
Case II – volume	0.653 m^3
Case III – volume	0.631 m^3
Inlet diameter	0.0215 m
Outlet diameter	0.0125 m
Weir height	0.35 m
Dam height	0.20 m

In addition, three new case studies were performed, namely, case I (actual bare tundish), case II (tundish with dam), and case III (tundish with dam and weir). Fig. 1 shows the computational domain for case III. In addition, an unstructured mesh for the same case, which is composed of tetrahedral and prism elements, is also depicted in the same figure.

Table 2 shows the operating physical parameters for the actual tundish configuration (case I) in addition to the proposed changes in tundish geometry by adding dam (case II), and dam and weir (case III).

3.2. *Solution procedure*

In ANSYS CFX, the mass and momentum equations are solved coupled for pressure and velocity components using the Element-based Finite-Volume Method (EbFVM). After solving the aforementioned variables, the turbulence model and energy equation are solved using a segregated approach. After the velocity and pressure fields reach the steady-state regime and for non-isothermal simulation, the energy equation does the same, the concentration equation, as well as the inclusion trajectory equation, is solved to obtain the tracer behavior into the tundish and the particle trajectory, respectively. The algebraic system of linear equations obtained after discretization is solved by using an algebraic multigrid methodology called the additive correction multigrid method [21]. Convergence was achieved when the root-mean-square (RMS) residuals were equal or smaller than 10^{-5} for mass, momentum and turbulence equations, and 10^{-6} for tracer advective-diffusion and energy equations.

4. Results and discussions

4.1. *Independence tests for the grid, time, and number of injected particles*

Independence tests for the grid, time, and a number of particles injected at the inlet were performed for each case study. By taking advantage of the geometry symmetry only half tundish is chosen for all simulation cases, except for the validation of case I, where a quarter of the geometry was used due to the presence of two symmetry planes. A mesh refinement study based on mean residence time, well-mixed volume, and dead volume is employed for all case studies. In this study, six types of non-uniform meshes composed of tetrahedral and prism elements were used, assuming a range of number of nodes varying from 4000 through 120,000. In Fig. 2, a mesh refinement study for case I using the SST model is shown.

From the results presented, it can be concluded that for meshes with more than 41,000 nodes the mean residence, well-mixed volume, and dead volume do not show any significant variation; therefore, the number of nodes chosen for case studies I, II, and III are equal to 64,000, 65,000, and 66,000, respectively.

A study of timestep convergence on the RTD curves for all case studies is also performed. Four different timesteps, ranging from 10 s through 0.01 s, were evaluated. Fig. 3 presents a timestep convergence study for case study II using the SST model.

Since the difference between the RTD curves with timesteps of 0.01 and 0.1 s were relatively small and aiming to avoid excessive computational time, we adopted the timestep of 0.1 s to represent all case studies presented in this work.

An independence test to quantify the total amount of particles, which simulates the non-metallic inclusions inserted at

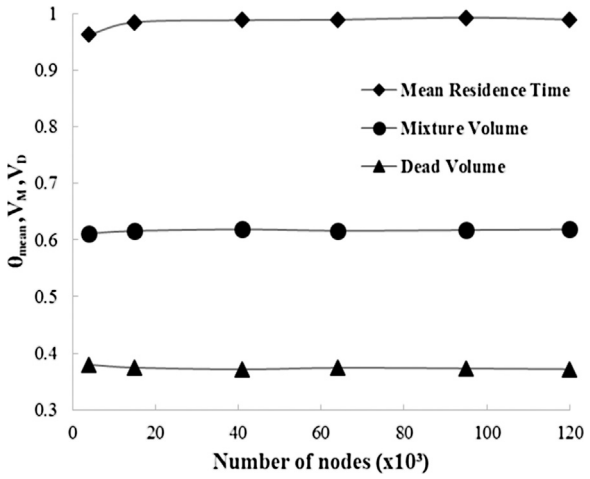

Fig. 2 – Mesh refinement study for the case I using SST model.

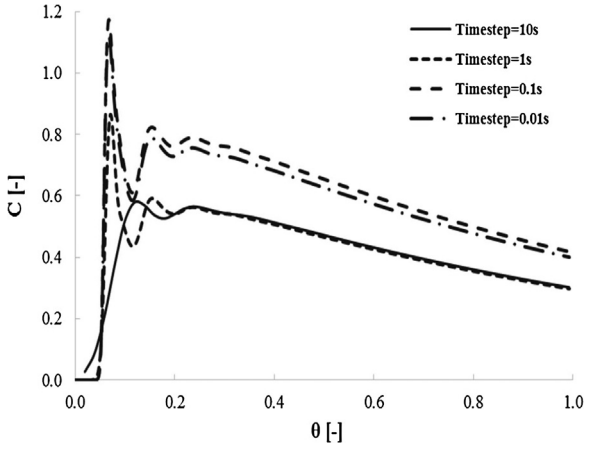

Fig. 3 – Timestep convergence for case II using SST model.

the inlet of the tundish region was performed for all case studies. Particle diameters of 5, 50, and 100 were employed, and a number of particles ranging from 20 to 10,000 particles were also employed for each particle diameter. For Lagrangian analysis, only the situation with the insertion of the Random Walk Model (RWM) was evaluated. The fraction of removed particles at the slag layer for case III, with the RWM, is presented in Fig. 4.

It can be concluded that the difference between the fraction of removed particles at slag layer with 1000 and 10,000 particles was minor; therefore, once again to avoid the excessive computational time, we chose 1000 particles to represent all case studies presented in this work.

4.2. *Validation case I*

Validation case I was performed by comparing the present work using two turbulence models with the experimental work of Kemeny et al. [7]. This validation was made by comparing the minimum and mean residence time from the present work and the experiments of the aforementioned work. The

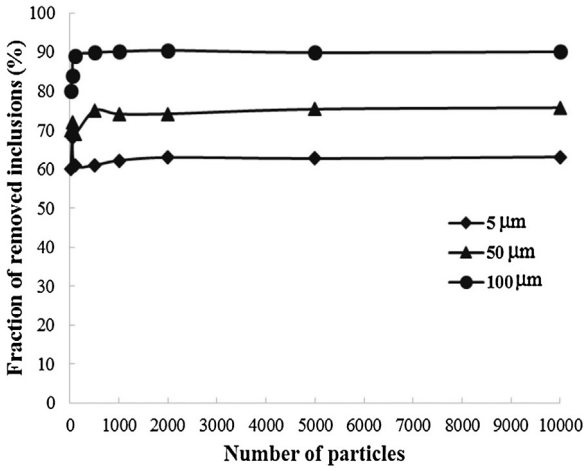

Fig. 4 – Independence test for case III with the RWM.

Table 3 – Comparison with experimental and numerical analyses – validation case I.

	θ_{min}	θ_{mean}
k–ε model – present work	0.097	0.959
SST model – present work	0.104	0.951
Kemeny et al. [7] – physical modeling	0.070	0.800
Daoud [25] – numerical modeling	0.130	0.920

results are presented in Table 3. As Daoud [27] performed the same analysis, we also present the numerical results obtained by him to further enhance the validation.

The results showed an acceptable agreement (from the engineering viewpoint) with both physical and numerical modeling from the literature. When comparing the efficiency between the two turbulence models, both of them showed similar results. While the k–ε turbulence model presented closer values for the minimum residence time, the SST turbulence model pointed out a better approximation for the mean residence time.

4.3. *Validation case II*

The validation case II was performed by comparing the numerical results of this work using two turbulence models with the experimental work of Wollmann [8]. For this validation case study, we compare the RTD curves as well as the minimum and mean residence time from the present work with the experimental results of Wollmann [8]. The results are shown in Fig. 5.

As it can be seen from Fig. 5, both turbulence models showed an acceptable agreement with the experimental work from the literature. Again, by comparing the accuracy between the two turbulence models, both of them showed similar results. However, if we carefully analyze the RTD curves for the central exit nozzle, the SST turbulence model showed better adjustment for the concentration peak. Therefore, for this T-delta-shaped tundish, the SST turbulence model seems to be a better choice for characterizing the turbulence quantities.

Finally, it is worth mentioning that despite of both turbulence models were able to predict the concentration peak of

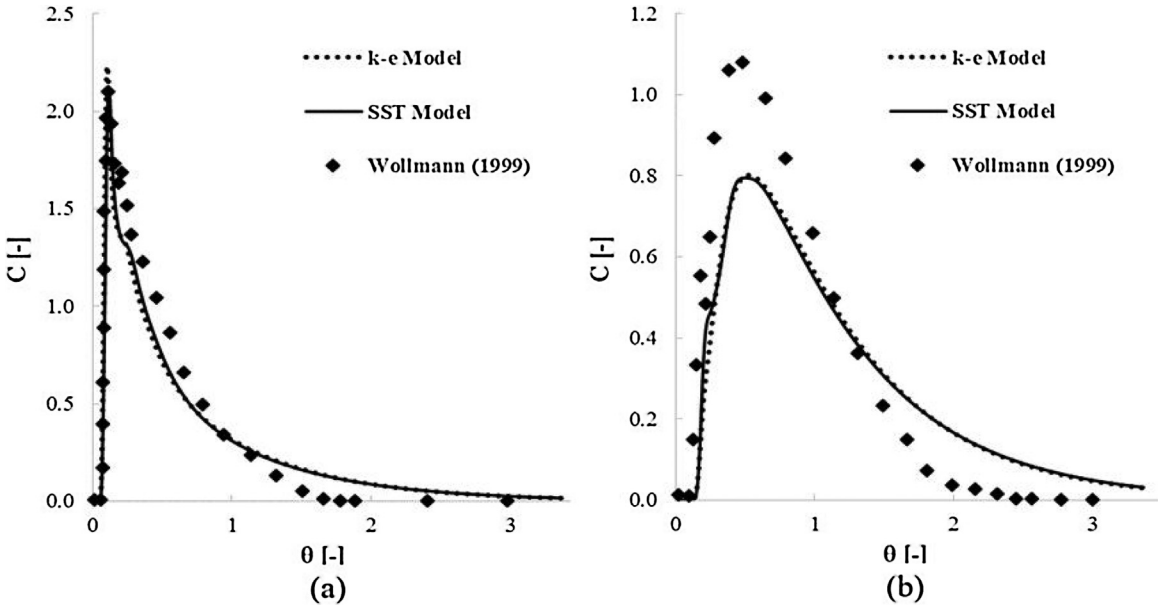

Fig. 5 – Comparison with experimental data for validation case II: (a) central exit nozzle and (b) lateral exit nozzle.

Table 4 – Comparison with experimental and numerical analyses – validation case II.

	θ_{min}	θ_{mean}
k–ε model – present work	0.125	0.954
SST model – present work	0.129	0.954
Wollmann (1999) – physical modeling	0.102	0.700
Daoud (2006) – numerical modeling	0.165	0.910

the RTD curves, they showed difficult to capture it properly in the RTD for the lateral exit nozzle. Table 4 compares the minimum and mean residence time extracted from the RTD curves showed in Fig. 2. The results from Daoud [27] were also included to enhance the validation.

Herein, the results from the present numerical simulation using both turbulence models predicted both minimum and mean residence time with good accuracy, when compared with experimental and numerical results from the literature. Again, when comparing the efficiency between the two turbulence models, both of them showed similar results. Therefore, taking into account these two characteristic times, both turbulence models can be used for representing the fluid flow into the investigated tundish.

4.4. *Validation case III*

For validating the Lagrangian analysis, the SST turbulence model was used. For this validation case, the path of the particles, which simulate the non-metallic inclusions traveling into the tundish is tracked. Two different cases were considered. The first one does not take into account the turbulence dispersion; the second, on the other hand, takes into account the use of the Random Walk Model (RWM) to simulate the chaotic effect of the turbulent eddies on the inclusion path.

Fig. 6 presents the total amount of removed inclusion at the slag layer. Fig. 6(a) does not consider the use of the RWM, whereas Fig. 6(b) presents the results by adding the RWM. From Fig. 6, it is clear that when the RWM is used more inclusions can be removed. Finally, the numerical results showed an acceptable agreement for both cases.

Considering that the results presented an acceptable agreement with both experimental and numerical analysis for all validation cases, and that the discrepancy between the comparisons can be attributed to some assumptions and the inherent deviation of the numerical studies from experimental ones, the methodology can be employed for the analysis of the actual tundish of a local steelmaker company. In addition, as both turbulence models presented similar results when the methodology was validated, we chose the SST turbulence model for the other numerical simulations.

4.5. *Case studies for isothermal analysis*

After validating the numerical methodology, the continuous casting tundish employed at a local steelmaker company was studied (case I – bare tundish). Furthermore, two more cases were performed to try to ameliorate the steel quality (case II – tundish with dam and case III – tundish with dam and weir).

4.5.1. *Flow field for the three case analysis*

Fig. 7 shows the predicted velocity fields at different planes for the three case studies. For the sake of visualization, the figures depicting the inlet and outlet longitudinal planes show only half of the tundish.

When we consider the actual tundish configuration (case study I), we can see in Fig. 7 (a), at the inlet longitudinal plane, that a high turbulent jet from the inlet reaches the bottom of the tundish and spreads toward the outlet region. Once there is no baffle for this case, this spreading goes directly to the outlet region, which will probably cause the appearance of short-circuiting flow and the presence of inclusions at outlet nozzles. From the set on the middle of the Fig. 7, when we add

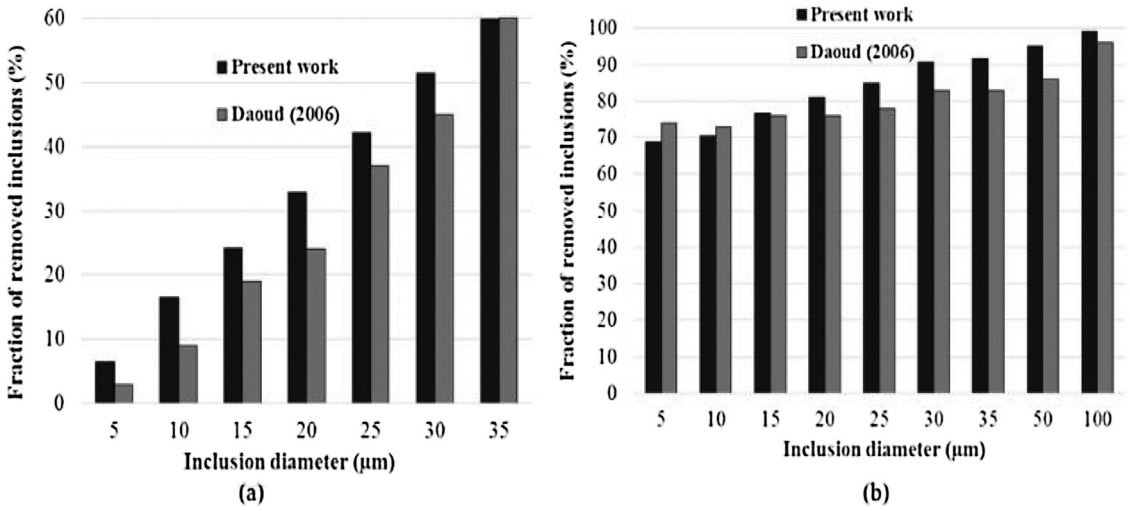

Fig. 6 – Comparison with numerical: (a) no RWM and (b) with RWM.

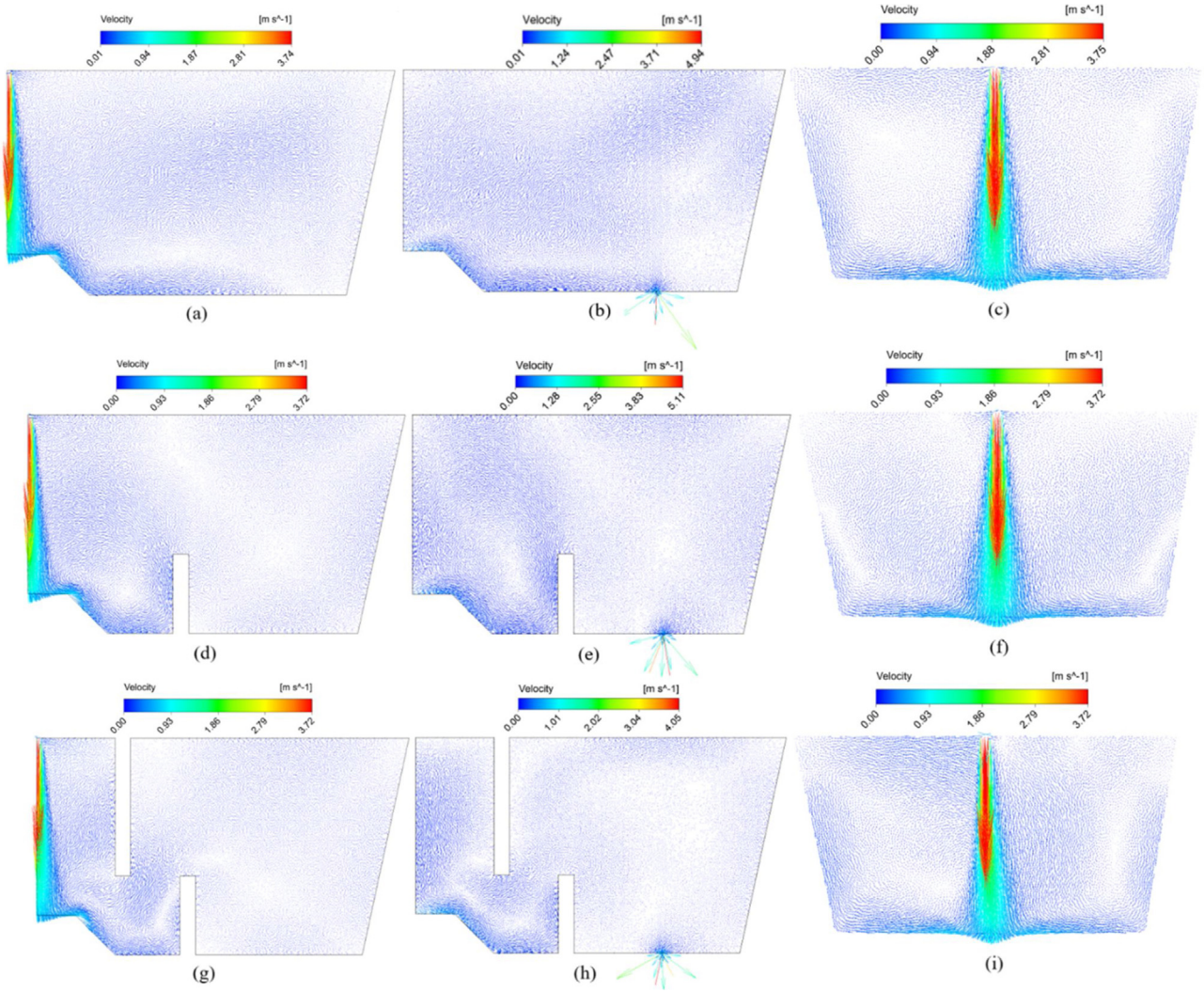

Fig. 7 – Isothermal flow pattern for case studies I, II, and III. (a, d, and g) Inlet longitudinal plane; (b, e, and h) outlet longitudinal plane; and (c, f, and i) inlet transverse symmetry plane.

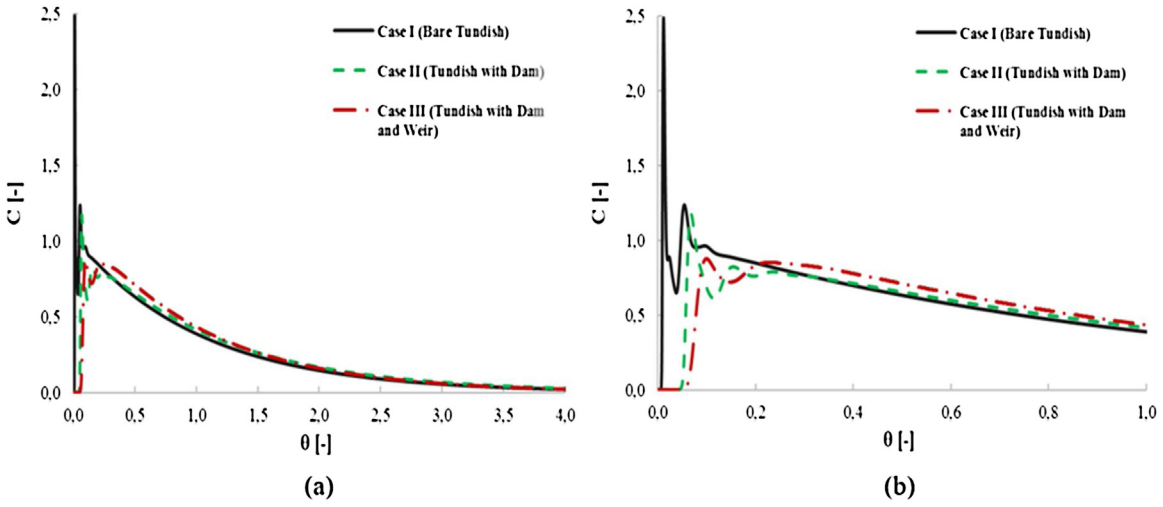

Fig. 8 – Comparison of the three cases – isothermal analysis: (a) RTD curves for the whole simulation time and (b) RTD curves showing the concentration peaks.

dams to the actual tundish (case study II), the turbulence is confined at inlet regions, and the flow modifiers do not allow the incoming fluid to go directly to the outlet region. Moreover, by adding dams, recirculating zones appear in the same region, and this fact may improve the mixing extent, which may also lead to a better homogeneous mixture to the final product. However, these recirculating zones may also cause a decreasing in mean residence time and dispersed plug flow volume. When weirs are added along with dams (case study III), similar conclusions verified to the case with only barriers are observed (see, for instance, Fig. 7(g)–(i)). In addition, as one can see in Fig. 7(i) higher values of mixing extent may appear, owing to the presence of high-velocity values at the inlet transverse symmetry plane. Finally, by comparing the magnitude of the velocity vectors at the outlet region, one can conclude that the insertion of flow modifiers decreased these values, which allows the flow to be more quiescent and does not carry inclusions for the following stages of the process.

4.5.2. *RTD parameters for the three case studies*

Fig. 8 shows the RTD curves for three case studies investigated, where they are confronted with each other to obtain a better configuration for improving the steel quality. This may be achieved by offering high values for both minimum and mean residence time.

For case I, a higher initial concentration peak is observed. This characterizes the existence of short-circuiting volume, which promotes the carrying of non-metallic inclusions toward the exit nozzles and then affecting the final steel quality. Also, this concentration peak appears early, which may carry inclusions from the inlet nozzle directly to the outlet nozzles. In addition, it is observed that once flow control modifiers are introduced, this undesirable volume drastically decreased; with the addition of weirs, this undesirable volume almost vanishes. Also, the absence of short-circuiting can be visualized as the C-curves present a significant displacement when the three cases are compared, indicating that the first fluid elements are spending more time into the vessel until they exit the tundish, which promotes an increase in the minimum and mean residence time.

Table 5 – Minimum and mean residence time for each configuration – isothermal analysis.

Case	θ_{min}	θ_{mean}
I	0.0078	0.989
II	0.051	1.12
III	0.062	1.08

Table 6 – The volume fraction of flow – isothermal analysis.

Case	Dead volume (%)	Dispersed plug volume (%)	Well mixed volume (%)
I	37.30	0.99	61.71
II	32.96	5.94	61.10
III	30.98	8.12	60.90

The results presented in Table 5 corroborate the previously observed results. From this table, we can observe that both minimum and mean residence time for fluid elements into the tundish increase when the flow modifiers are added, which is very important for steel cleanliness once inclusions have more time to float out, and consequently the inclusions can be captured by the slag layer.

Furthermore, to improve the steel quality, dead volume needs to be minimized, dispersed plug volume maximized, and well-mixed volume is kept in a suitable value [3]. Table 6 shows that these requirements have been achieved as long as one makes use of the flow modifiers. As expected, a better performance was achieved for the case study III, where the combination of dams and weirs showed the best efficiency. Hence, the use of flow control devices has been justified.

The use of the Random Walk Model (RWM) to simulate the chaotic turbulent effects is considered to be more representative of the turbulent state in an actual tundish [25]. As a result, all the results shown next were performed by taking into account the RWM. Fig. 9 shows the fraction of captured

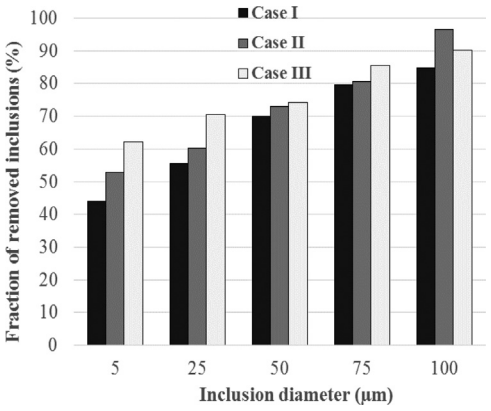

Fig. 9 – Lagrangian analysis for the three cases with RWM – isothermal analysis.

inclusions at the slag cover as a function of a range of particle diameters.

From Fig. 9, it is clear that the larger the diameter of the inclusions is, the higher is the efficiency of the inclusions removed. This was already expected since inclusions with large diameters tend to be more susceptible to float out and to be captured by the slag layer through buoyancy force mechanism. Also, for the whole range of inclusion diameter, the addition of flow control devices enhances the inclusion removal at the slag layer. The combination of dams and weirs shows the best efficiency with all particle diameter, except with the largest particles, where the configuration with just dams had a better performance.

4.6. *Case studies for non-isothermal analysis*

As previously mentioned, for all cases, the SST turbulence model was used.

4.6.1. *Temperature field for the three case studies*

Fig. 10 depicts the temperature distribution in specified planes of the investigated tundishes.

From Fig. 10(a)–(c), the case study I, it can be seen that the hottest molten steel is concentrated at the inlet region, while the bulk fluid region presents regions of lower liquid steel temperature. This can be considered a favorable situation to promote fluid homogenization. Furthermore, the coolest molten steel occurs at the corner of the tundishes, where dead regions are also present. This is an undesirable situation since the more the molten steel stays in these regions, the more is the chance to the liquid steel solidifies into the tundish and not be carried to the molds. Fig. 10(d)–(f) shows the temperature profiles at different planes for the case study II. From the figure it is noticeable that by inserting dams, the hottest molten steel is concentrated in a broader region than it was for the case study I. This situation favors the mixing of the hot inlet jet provided by the ladle and the existing fluid into the

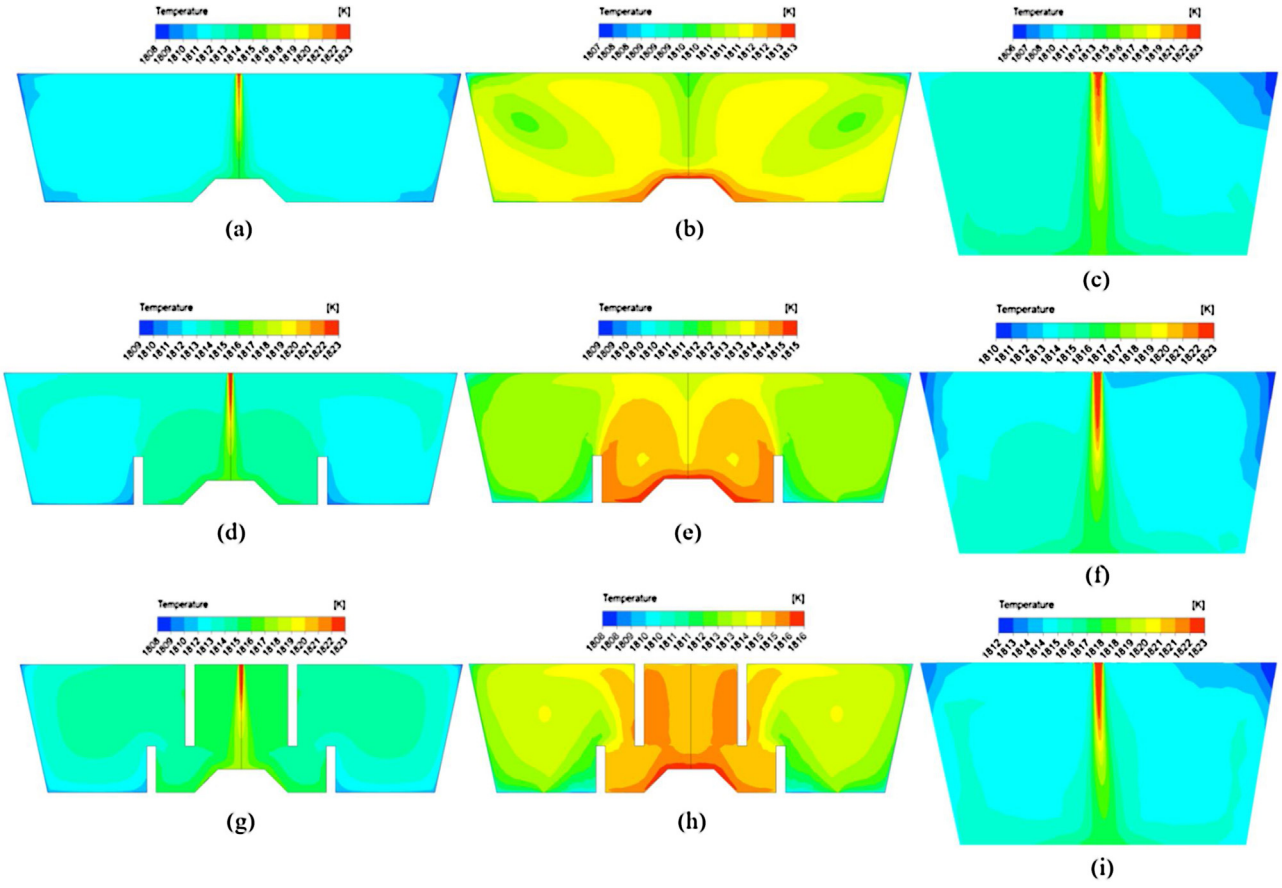

Fig. 10 – Temperature contours for case studies I, II, and III: (a, d and g) inlet longitudinal plane; (b, e and h) outlet longitudinal plane; and (c, f and i) inlet transverse symmetry plane.

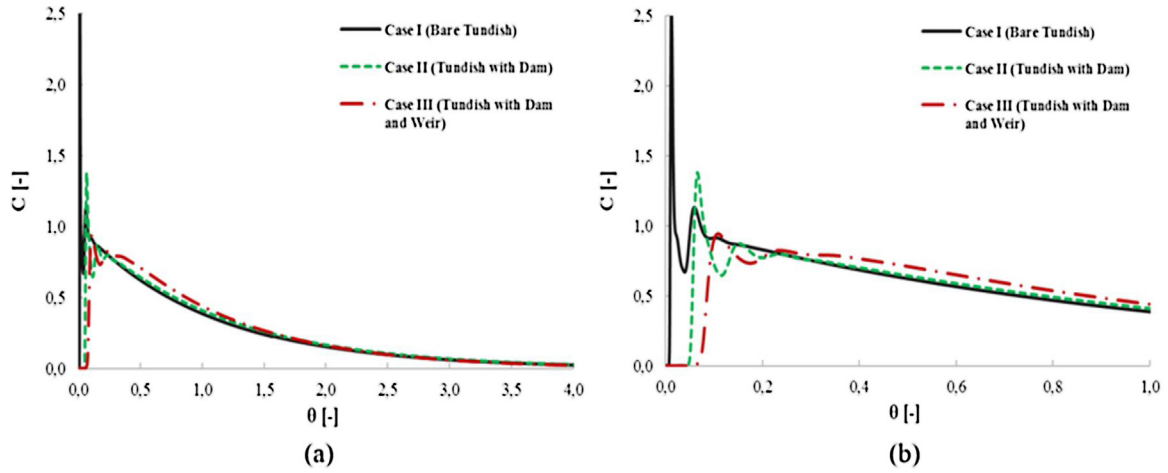

Fig. 11 – Comparison of the three cases – non-isothermal analysis: (a) RTD curves for the whole simulation time and (b) RTD curves showing the concentration peaks.

Table 7 – Minimum and mean residence time for each configuration – non-isothermal analysis.

Case	θ_{min}	θ_{mean}
I	0.008	1.029
II	0.05	1.115
III	0.07	1.092

Table 8 – The volume fraction of flow – non-isothermal analysis.

Case	Dead volume (%)	Dispersed plug volume (%)	Well mixed volume (%)
I	37.03	1.03	61.94
II	33.65	5.80	60.55
III	30.47	9.07	60.46

tundish. However, by adding dams it is created cooler regions behind them, and also cooler regions are increased at the inlet of the transversal symmetry plane. Fig. 10(g)–(i) presents the temperature field for the case study III. From this figure, by inserting weirs, the inlet region increases the concentration of the hottest molten steel. In addition, cooler regions presented at corners and behind dams seem to be reduced significantly.

4.6.2. *RTD parameters for the three case studies*

The RTD curves for all the non-isothermal cases as wells as the characteristic times and volumes are presented in Fig. 11, Table 7, and Table 8, respectively.

As we can see from these results, there is no significant difference between the results achieved with isothermal and non-isothermal studies. Therefore, similar considerations can be drawn for both analyses, and for the sake of simplicity, they will not be repeated here. Also, the results obtained in the present work did not present expected differences when comparing some aspects of both isothermal and non-isothermal simulations, for instance, different RTD curves [14]. However, this fact may be attributed to the fact that the tundish volume employed by Alizadeh et al. [13] was about twice larger than the tundish employed in the present work.

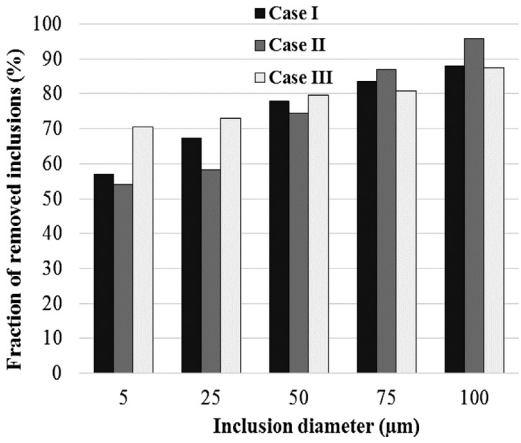

Fig. 12 – Lagrangian analysis for the three cases with RWM – non-isothermal analysis.

4.6.3. *Lagrangian analysis for the three case studies*

Fig. 12 shows the fraction of removed inclusions at the slag layer for the non-isothermal case.

Unlike the Eulerian analysis for the isothermal and non-isothermal case, the Lagrangian analysis showed different results when comparing the number of particles removed at the slag layer. As expected, the presence of buoyancy forces increased the removal of non-metallic inclusions. Also, considering small particles, the case study III appears to be the best configuration to adopt, whereas for large particles, namely, particles with diameters of 75 and 100 μm, the case study II presented a better efficiency of removal. The results showed here are by the work of Miki and Thomas [18].

5. Conclusions

In the present work, a methodology has been developed able to determine optimal configuration, which enhances the steel cleanliness in an actual steel continuous casting tundish

plant. The results using the model approach presented a good agreement with experimental data, validating the calculations, and allowing further scenarios investigation.

Based on the analysis, the flow control devices inserted into the actual tundish operation enhanced the reactor operation by increasing the minimum and mean residence time, allowing for increasing the cleanness of the steel. Furthermore, considering the Lagrangian analysis, the fraction of removed inclusions at the slag covering layer increased with the use of these flow modifiers.

Therefore, the use of such flow control devices provides an efficient and reliable way to promote inclusion flotation toward the slag layer to capture and remove them and consequently promotes the enhancement of steel cleanliness.

Finally, by confronting all case studies, we indicated that by simply adding dams the steel cleanness can significantly be enhanced and for some specific cases analyzed this simply addition showed better performance when compared with the introduction of dams in conjunction with weirs. Nevertheless, in general, better flow pattern and inclusion remotion rates are obtained by combining dams and weirs (case III).

Conflicts of interest

The author declares no conflicts of interest.

Uncited references

[22,26].

Acknowledgments

The authors would like to thank the financial support provided by CNPq (The National Council of Technological and Scientific Development) and the local steelmaker company for making available the actual tundish parameters. This study was also financed in part by the Coordenação de Aperfeiçoamento de Pessoal de Nível Superior – Brasil (CAPES).

REFERENCES

[1] Gardin P, Brunet M, Domgin JF, Pericleous K. An experimental and numerical CFD study of turbulence in a tundish container. Appl Math Model 2002;26:323–36.
[2] Sahai Y, Ahuja R. Steel flow and mixing of melt in steelmaking tundishes; 1986.
[3] Wang G. Flow mechanism of molten steel in a single-strand slab caster tundish based on the residence time distribution curve and data; 2015.
[4] Kumar A, Koria SC, Mazumdar D. An assessment of fluid flow modelling and residence time distribution phenomena in steelmaking tundish systems. ISIJ Int 2004;44:1334–41.
[5] Maliska CR. Heat transfer and computational fluid mechanics. 2nd ed. Rio de Janeiro: LTC; 2004 [in Portuguese].
[6] Mazumdar D, Guthrie RIL. The physical and mathematical modelling of continuous casting tundish systems. ISIJ Int 1999;39:524–47.
[7] Kemeny F, Harris DJ, MClean A, Meadowcroft TR, Young JD. Fluid flow studies in the tundish of a slab caster. Process Technol Conf 1981;2:232–45.
[8] Wollmann AM. Flow studies in a continuous casting tundish. In: Graduate program in mining, metallurgical and materials engineering. Porto Alegre: Federal University of Rio Grande do Sul; 1999 [in Portuguese].
[9] Chen C, Ni P, Jonsson LTI, Tilliander A, Cheng G, Jönsson PG. A model study of inclusions deposition, macroscopic transport, and dynamic removal at steel–slag interface for different tundish designs. Metal Mater Trans B 2016;47:1916–32.
[10] Ding N, Bao Y-p, Sun Q-s, Wang L-f. Optimization of flow control devices in a single-strand slab continuous casting tundish. Int J Miner Metal Mater 2011;18:292–6.
[11] Ray SK. On the application of physical and mathematical modeling to predict tundish performance. Canada: McGill University; 2009.
[12] Sheng DY, Jonsson L. Investigation of transient fluid flow and heat transfer in a continuous casting tundish by numerical analysis verified with nonisothermal water model experiments. Metal Mater Trans B 1999;30:979–85.
[13] Alizadeh M, Edris H, Shafyei A. Fluid flow and mixing in non-isothermal water model of continuous casting tundish. J Iron Steel Res Int 2008;15:7–22.
[14] De Kock DJ. Optimal tundish design methodology in a continuous casting process. Pretoria: University of Pretoria; 2005.
[15] Szekely J, Ilegbusi OJ. The physical and mathematical modeling of tundish operations. New York: Springer-Verlag; 1989.
[16] Raghavendra K, Sarkar S, Ajmani SK, Denys MB, Singh MK. Mathematical modelling of single and multi-strand tundish for inclusion analysis. Appl Math Model 2013;37:6284–300.
[17] Sowa L. Effect of steel flow control devices on flow and temperature field in the tundish of continuous casting machine; 2015.
[18] Miki Y, Thomas BG. Modeling of inclusion removal in a tundish. Metal Mater Trans B 1999;30:639–54.
[19] Bensouici M, Bellaouar A, Talbi K. Numerical investigation of the fluid flow in continuous casting tundish using analysis of RTD curves. J Iron Steel Res Int 2009;16:22–9.
[20] Zheng S, Zhu M, Zhu Y, Su W. Flow characteristics and inclusion removal in a ten-strand continuous casting tundish: physical modeling and industrial trials. J Iron Steel Res Int 2016;23:92–7.
[21] CFX. User's guide for ANSYS CFX Release 14.0, USA; 2011.
[22] Launder BE, Spalding DB. The numerical computation of turbulent flows. Comput Meth Appl Mech Eng 1974;3:269–89.
[23] Menter F, Ferreira JC, Esch T, Konno B. The SST turbulence model with improved wall treatment for heat transfer predictions in gas turbines; 2003.
[24] Thomas BG, Yuan Q, Mahmood S, Liu R, Chaudhary R. Transport and entrapment of particles in steel continuous casting. Metal Mater Trans B 2014;45:22–35.
[25] Crowe C, Sommerfeld M, Tsuji Y. Multiphase flows with droplets and particles. New York/London: CRC Press; 1998.
[26] Vargas-Zamora A, Morales RD, Diaz-Cruz M, Palafox-Ramos J, Garcia Demedices L. Heat and mass transfer of a convective-stratified flow in a trough type tundish. Int J Heat and Mass Transfer 2003;46:3029–39.
[27] Daoud ILA. Numerical study of the flow and behavior of non-metallic inclusions in steel continuous casting tundishes. In: Graduate program in mining, metallurgical and materials engineering. Porto Alegre: Federal University of Rio Grande do Sul; 2006 [in Portuguese].
[28] Bejan A. Heat transfer. New York: John Wiley & Sons; 1993.